Polyamorphism and the evolution of intermediate-range order in molten $ZnCl_2$

2008 J. Phys.: Condens. Matter 20 244123

(http://iopscience.iop.org/0953-8984/20/24/244123)

J. Phys.: Condens. Matter **20** (2008) 244123 (9pp) doi:10.1088/0953-8984/20/24/244123

Polyamorphism and the evolution of intermediate-range order in molten $ZnCl_2$

Bevan K Sharma[1] **and Mark Wilson**[2]

[1] Department of Chemistry, University College London, 20 Gordon Street, London WC1H 0AJ, UK
[2] Department of Chemistry, Physical and Theoretical Chemistry Laboratory, University of Oxford, South Parks Road, Oxford OX1 3QZ, UK

Received 13 December 2007, in final form 28 January 2008
Published 29 May 2008
Online at stacks.iop.org/JPhysCM/20/244123

Abstract
The pressure- and temperature-dependent properties of molten zinc chloride are investigated by means of molecular dynamics computer simulation. The potential model used is based on a pair potential augmented with a description of the (many-body) anion polarization. The static experimental and simulated structural properties are briefly reviewed. The structural properties obtained from the simulation model are compared with those obtained from experimental investigations and trends with the change in system pressure and temperature are discussed. Preliminary studies of the pressure behaviour of the simulated glassy states show the existence of low-and high-density amorphous states (LDA and HDA). The LDA/HDA coexistence line is established and its relationship to the underlying phase diagram is discussed.

1. Introduction

Molten salts are well known as displaying highly organized (ordered) structures to extremes of temperature and pressure, the origin of which lies in the presence of strong electrostatic forces [1–4]. In addition, such systems may show ordering on length-scales beyond those easily associated with the electrostatic (anions surround cations and *vice versa*) ordering. As a result, a potentially useful classification is that of the *network* liquid or glass. In the MX_2 stoichiometry, for example, systems such as SiO_2 and BeF_2 can be considered as constructed from purely corner-sharing local MX_4 coordination tetrahedra, whilst $SiSe_2$ and $BeCl_2$ can be considered as constructed from purely edge-sharing units. The classification of systems in this manner has implications beyond simply understanding the nature of the underlying static structure. For example, a purely corner-sharing network percolates in three dimensions and, as a result, would be expected to have a relatively high melting point and be relatively rigid in structure. On the other hand, structures constructed by percolating purely edge-sharing tetrahedra produce chains which are charge neutral and, as a result, these systems can be considered as ensembles of polymer-like pseudo-one-dimensional chains, the forces between which are dominated by relatively weak multipolar and van der Waals interactions [5]. The relative weakness of these interactions promotes relatively low melting points and a greater structural flexibility with respect to the more rigid three dimensional networks. In many ways, therefore, the most interesting cases are systems in which both corner- and edge-sharing units appear. Two systems are particularly worthy of note in this context; $ZnCl_2$ and $GeSe_2$. Both systems have been studied extensively theoretically [6–8] and experimentally [9–11]. The construction of simulation models for $GeSe_2$ is, however, hampered by the inherent structural complexity, namely the presence of nearest-neighbour like–like (homopolar) atom pairs [9, 10]. This structural complexity renders the use of a purely ionic description controversial [12]. $ZnCl_2$, however, appears to show no such like–like interactions and, as a result, an ionic description appears appropriate with little controversy. In simple static structural terms $ZnCl_2$ represents an 'intermediate' case between the purely edge- and corner-sharing extrema, in the sense that the mean Zn–Cl–Zn bond angle of $\sim$110° [13] allows for both edge- and corner-sharing units.

The total structure factors obtained experimentally show the presence of a so-called first-sharp diffraction peak (FSDP) or 'prepeak' at scattering angles corresponding to $k \sim 1$ Å^{-1} [14–17] which is generally considered as dominated by intermediate-range order (IRO) present in the cation sub-density (and hence resolved primarily to the $S_{ZnZn}(k)$ partial structure factor, although this viewpoint has been challenged [17]). Previous work has shown how such IRO can be rationalized [18, 19]. In a simple rigid-ion representation

of the inter-ionic interactions in which the system is an ensemble of ions which carry their formal ionic charges, the cation–cation nearest-neighbour separation is longer than the corresponding anion–anion length-scale, simply reflecting the greater formal charge present on the cation (and which leads to the relatively obtuse M–X–M bond angle). The inclusion of anion dipole polarization acts to reduce the M–X–M bond angle with respect to the rigid-ion limit as a dipole is induced on the inter-tetrahedral bridging anion which acts to introduce negative charge to in between the two cations, and hence effectively screens their repulsive Coulombic interaction. The overall result is to reduce the nearest-neighbour cation–cation separation (in $ZnCl_2$ to approximately that of the anion–anion pair [14]) which in turn leads to a depletion of cation density on an intermediate length-scale.

Clearly, changes in both temperature and pressure may be expected to influence the underlying network topology. To this end, the application of pressure represents perhaps the most direct and accessible method for inducing large-scale changes in the inherent network topology. On compression the network topology alone may change (retaining the underlying linked tetrahedron motif) and/or the ion coordination number may increase. These changes have profound implications for the IRO and for any potential polyamorphism. However, the technical difficulties inherent in carrying out high pressure experimental investigations effectively precludes information being obtained directly regarding the partial structure factors. As a result, computer simulation models may provide invaluable insight into pressure-driven structural changes.

The presence of IRO may have profound implications for the system properties. For example, the ion dynamics on the intermediate length-scale may slow down more dramatically than those associated with the nearest-neighbour length-scale. As a result, the system dynamics, on cooling to the glass transition temperature, may become dominated by relaxations associated with the intermediate length-scale [20]. In addition, these system may have properties which lead to readily-observable polyamorphic behaviour. The presence of liquid–liquid phase transitions, driven in pure materials by changes in density and/or entropy, remains a 'hot' topic [21–26]. In this context, $ZnCl_2$ can be considered as a tetrahedral network and hence analogous to H_2O [27, 28], SiO_2 [29] and GeO_2 [30]. However, the network in $ZnCl_2$ can be considered as 'less open' (more acute inter-tetrahedral bond angles) than these systems and so it is unclear how any underlying polyamorphism may appear. $ZnCl_2$ may, indeed, represent a useful system for the direct observation of the polyamorphism as the underlying pressure-driven crystalline phase transitions occur at relatively low pressures compared to those in SiO_2 or GeO_2. Both SiO_2 and GeO_2 can be compressed into densified structures, which are recoverable to ambient conditions, under the application of pressure [31] or by irradiation [32], the structure of which can be understood in terms of subtle rearrangements on the intermediate length-scale [33, 34]. Simulation studies on SiO_2, for example, indicate a change in local ion coordination implying the presence of low- and high-density states [35].

In this paper we investigate the structural behaviour of a potential model which describes $ZnCl_2$ on the application of pressure and temperature. We will pay particular attention to a direct comparison with experimental data with reference to the evolution of the signatures of IRO. Finally, we will make some preliminary predictions regarding possible underlying polyamorphic behaviour.

2. Experimental background

The experimental study of the static structure of both molten and glassy $ZnCl_2$ has a relatively long history, possibly reflecting the relatively low ambient pressure melting point ($T_m = 591$ K). Early diffraction studies focused on the ambient pressure liquid (x-rays [36, 37], neutrons [14, 15, 38]) and glass (x-rays [39, 37], neutrons [13, 40, 38]). With the exception of the neutron diffraction study of Allen *et al* [15], which probed the structure of liquid $ZnCl_2$ at two temperatures, these early studies focused primarily on single p–T state points. More recent investigations have probed a range of pressure and temperature state points. EXAFS on the glass, liquid and crystalline states has highlighted the similarity of the local ion environments under ambient pressures [41]. X-ray diffraction studies on the liquid state up to pressures of ∼4 GPa [42] highlights the possibility of a change in the intermediate-range order at higher pressures, possibly as a result of a change in the local coordination number (analogous to the γ-$ZnCl_2 \longrightarrow CdCl_2$ four-to six-coordinate cation pressure-driven transformation observed in the crystalline state [43, 44]). High energy photon studies to pressures of ∼0.3 GPa [45] and ∼0.4 GPa [46] respectively indicate a loss in FSDP intensity on increasing pressure (again indicative of changes in the IRO).

A significant problem is obtaining information on a *partial* structure factor level (i.e. information regarding specific ion pair spatial correlations). For $ZnCl_2$, Biggin and Enderby [14] generated the three partial structure factors using chlorine atom isotopic substitution. These data has been recently re-analysed by Soper [47]. Salmon *et al* [16] have recently obtained partial structure factor information for the glassy state. In the absence of direct access to the partial structure factors, Neuefeind [17, 48] has combined the total scattering functions obtained from high energy photon and neutron studies to effectively eliminate a single structure factor (generating functions which are linear combinations of the two remaining partial structure factors). The same author [17] has also discussed the possible form of the partial structure factors themselves by eliminating a single partial and then assuming a detailed knowledge of an additional function ($S_{ZnCl}(k)$).

3. Computational background

Previous computational studies have highlighted the problems inherent in modelling $ZnCl_2$, despite its apparent high ionicity. Using a formal charge ionic Born–Mayer pair potential, Woodcock, Angell and Cheeseman reproduced the nearest-neighbour anion–cation separations and generated a linked tetrahedral network [49], but failed to reproduce the nearest-neighbour Zn–Zn separation and the associated relatively acute Zn–Cl–Zn bond angles. The same problem arose in

Table 1. Potential parameters used in the present work. The ion–ion interactions are modelled using a Born–Mayer potential in which the short-range interaction is given by $U(r_{ij}) = B_{ij}\exp(-a_{ij}r_{ij}) - C_{ij}^6/r_{ij}^6$.

ij	B_{ij} (au)	a_{ij} (au)	C_{ij}^6 (au)
ZnCl	43.72	1.600	43.7
ClCl	87.00	1.556	183.0
ZnZn	27.00	1.556	40.0

the work of Gardner and Heyes [50] despite testing models in which the ion charges were reduced from their formal (valence) values. Kumta *et al* [51] reproduced the Zn–Zn nearest-neighbour separation by increasing the Zn–Zn dipole–dipole dispersion interaction. However, the magnitude of the required dispersion coefficient, controlling this interaction in this potential model, $C_6^{\mathrm{ZnZn}} \sim 7200$ au, is significantly larger than that predicted using the *ab initio* cation polarizability ($\alpha_{Zn^{2+}} \sim 5$ au [52], giving $C_6^{\mathrm{ZnZn}} \sim 40$ au) using a Slater–Kirkwood formula [53]. This difference, coupled with the fact that the dispersive interaction is the only direct attractive interaction acting between cation pairs in models of this type, indicates that the enhanced dispersion may, in fact, be mimicking some critical missing physics (here the anion polarization—see below). Later work, for example, showed the ion dynamics displayed by this model to be very stiff compared with experiment [54]. Bassen *et al* [55] further support these ideas by using a modified (screened) Coulombic interaction to model the liquid over a range of temperatures. Huang *et al* [56] use a shell model (a particular mechanical representation of the ion polarizability) to similar ends.

4. Potential models

The potential model used has been described previously [57]. A Born–Mayer effective pair potential of the form

$$U(r_i j) = B_{ij}\mathrm{e}^{-a_{ij}r_{ij}} + \frac{Q_i Q_j}{r_{ij}} - \frac{C_6^{ij}}{r_{ij}^6}, \qquad (4.1)$$

is used, where B_{ij} and a_{ij} are represent the contribution of the ion radii to, and the rate of decay of, the repulsive wall, C_6^{ij} are the dipole–dipole dispersion parameters and $Q_i(j)$ is the (formal) charge on ion $i(j)$. The potential parameters are listed in table 1. The pair potential is augmented with a description of the anion dipolar polarization using a polarizable-ion model (PIM) [18]. The PIM requires two further parameters. The anion polarizability is taken as 20 au, consistent with both *ab initio* values [58] and experimentally-determined refractive indices (see [59] and references therein). The short-range damping parameter, which controls the short-range (nearest-neighbour) contributions to the anion dipole moments, is taken as 1.65 au, again consistent with *ab initio* values obtained from the consideration of anions in distorted crystalline environments [60]. A system size of 999 ions is used in order to maximize both accessible length- and timescales with the temperature and pressure maintained using Nosé–Hoover thermostats [61] and barostats [62] respectively. Statistical averages were taken over ∼1 ns over a temperature range of 600–1200 K and a pressure range of 0–0.3 GPa.

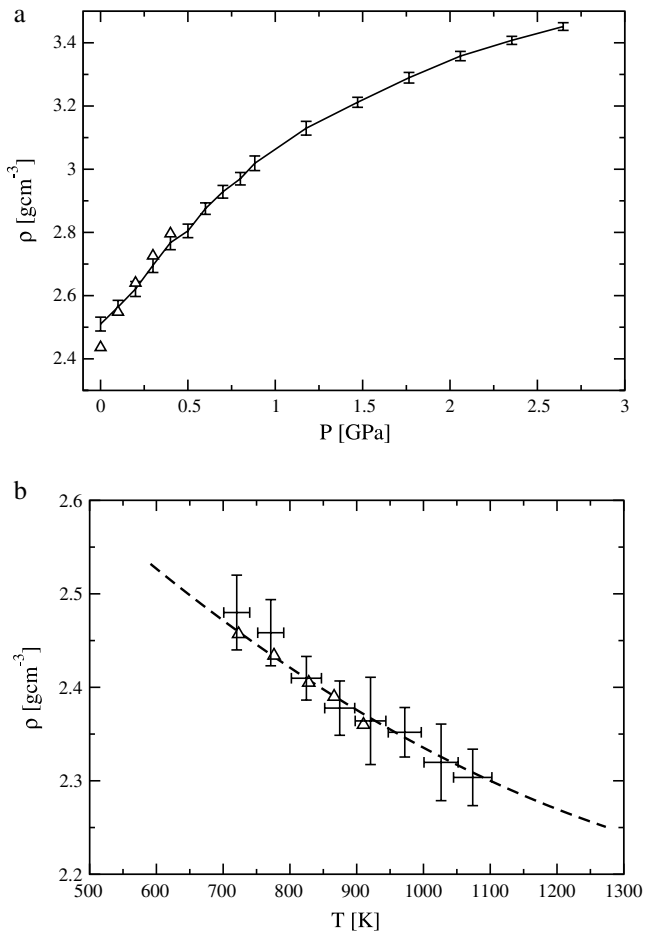

Figure 1. (a) Simulated system densities for the $T = 723$ K isotherm as a function of pressure (solid line). The points △ show the experimental densities [46]. (b) Simulated system densities for the zero pressure isochore. The points show the experimental densities from reference [64] and the dashed line the density equation from [63].

5. Results

5.1. Static structure

Figure 1(a) shows the simulated system density, calculated along the 723 K isotherm, as a function of pressure and compared to experimental values [46]. The simulated densities appear in good agreement with the experimental values. Figure 1(b) shows the density evolution as a function of temperature for the zero pressure isochore. Again, the calculated densities appear in good agreement with those observed experimentally [63, 64].

Figures 2(a) and (b) shows the calculated total neutron and x-ray diffraction patterns, $F^{\mathrm{nd}}(k)$ and $F^{\mathrm{xrd}}(k)$ as a function of pressure. Both functions are generated by calculating the Ashcroft–Langreth partial structure factors, $(S_{\alpha\beta}(k) = \langle A_\alpha^*(k) \cdot A_\beta(k)\rangle$, where $A_\alpha(k) = \frac{1}{\sqrt{N_\alpha}}\sum_{i=1}^{N_\alpha} \mathrm{e}^{\mathbf{i}\mathbf{k}\cdot\mathbf{r}_i}$ are the Fourier components. For the total neutron scattering function,

$$F^{\mathrm{nd}}(k) = c_\alpha b_\alpha^2 \left(S_{\alpha\alpha}(k) - 1\right) + c_\beta b_\beta^2 \left(S_{\beta\beta}(k) - 1\right) + 2(c_\alpha c_\beta)^{1/2} b_\alpha b_\beta \left(S_{\alpha\beta}(k)\right), \qquad (5.1)$$

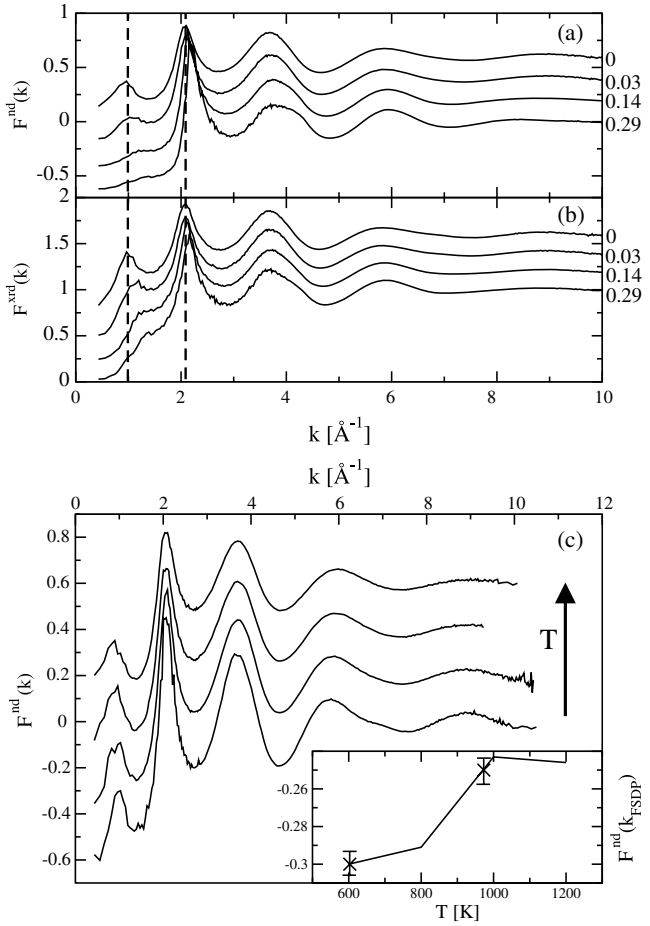

Figure 2. Total (a) neutron and (b) x-ray scattering functions obtained at four pressures (indicated on the right in GPa). Successive pressure lines are shifted by 0.2 along the y-axis for clarity. The vertical dashed lines at $k \sim 1$ Å^{-1} and $k \sim 2$ Å^{-1} are drawn as guides to the eye to allow the resolution of subtle shifts in the positions of both the principal peak and first-sharp diffraction peak. (c) Total neutron scattering functions as a function of temperature. The functions shown are (from bottom to top) generated at temperatures of 600 K, 800 K, 1000 K and 1200 K. The figure inset shows the intensities of the FSDPs compared to the experimental values from [15].

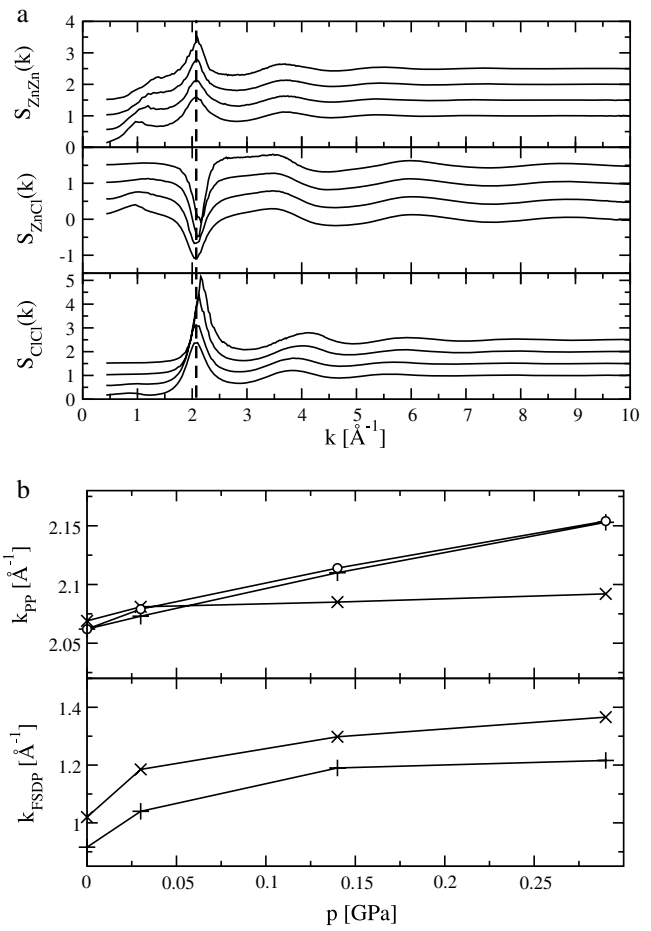

Figure 3. (a) Partial Ashcroft–Langreth structure factors calculated as a function of pressure (of 0.0, 0.03, 0.14 and 0.29 GPa from bottom to top in each panel). Each successive pressure curve is shifted by 0.5 along the y-axis for clarity. The vertical dashed line at $k \sim 2$ Å^{-1} is drawn to aid resolution of the shifts in the position of the principal peak. (b) Principal (upper panel) and first-sharp (lower panel) diffraction peak positions as a function of pressure. Key: ×—$S_{\mathrm{ZnZn}}(k_{\mathrm{X}})$, +—$S_{\mathrm{ZnCl}}(k_{\mathrm{X}})$, ○—$S_{\mathrm{ClCl}}(k_{\mathrm{PP}})$ (X = PP, FSDP).

where $c_{\alpha(\beta)}$ is the mole fraction of species $\alpha(\beta)$ and $b_{\alpha(\beta)}$ is the corresponding coherent neutron scattering length. For the total x-ray scattering function $b_{\alpha(\beta)}$ is replaced by the (k-dependent) form factor, $f_{\alpha(\beta)}(k)$. The neutron scattering lengths and x-ray form factors are taken from [65] and [66] respectively, the former corresponding to the natural (∼3:1) ^{35}Cl:^{37}Cl composition. At zero pressure both $F^{\mathrm{nd}}(k)$ and $F^{\mathrm{xrd}}(k)$ show a significant FSDP at $k \sim 1$ Å^{-1}. As the pressure increases the FSDP position shifts to higher k and its intensity systematically decreases consistent with experiment [42, 45, 46].

Figure 2(c) shows the total neutron function as a function of temperature. As the temperature is increased the height of the principal peak (at $k \sim 2$Å^{-1}) decreases in intensity (as is usual). However, the intensity of the FSDP rises as the temperature is increased. The figure inset shows that the observed change in intensity is consistent with experiment [15].

Figure 3(a) shows the Ashcroft–Langreth partial structure factors at the four pressures highlighted in figure 2. The FSDP is clear in the zero pressure $S_{\mathrm{ZnZn}}(k)$ and $S_{\mathrm{ZnCl}}(k)$ functions. The FSDP in $S_{\mathrm{ZnZn}}(k)$ mirrors the behaviour of both the x-ray and neutron total scattering functions in shifting to higher k (figure 3(b)) as the pressure is increased, with a corresponding reduction in intensity. In contrast, the FSDP in $S_{\mathrm{ZnCl}}(k)$, whilst shifted to higher k at the lower pressure increment (figure 3(b), mirroring the behaviour of $S_{\mathrm{ZnZn}}(k)$), near-vanishes at the higher pressures. The principal peaks in both $S_{\mathrm{ZnCl}}(k)$ and $S_{\mathrm{ClCl}}(k)$ show similar shifts in position to higher k as the pressure is increased (as shown in the upper panel of figure 3(b)). The principal peak in $S_{\mathrm{ZnZn}}(k)$, however, shows a distinctive behaviour with a small initial shift to higher k at low pressure, followed by an even smaller shift to higher k on further pressure increase.

Neuefeind *et al* [48] takes linear combinations of the high energy photon and neutron total structure factors in order to eliminate a single partial structure factor (defined by the ion

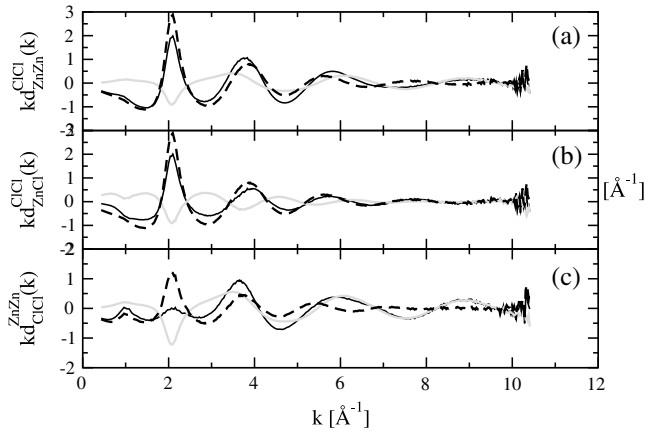

Figure 4. Functions obtained from the linear combination of the partial structure factors as constructed in [48]. (a) $kd^{\mathrm{ClCl}}_{\mathrm{ZnZn}}(k)$, (b) $kd^{\mathrm{ClCl}}_{\mathrm{ZnCl}}(k)$, (c) $kd^{\mathrm{ZnZn}}_{\mathrm{ClCl}}(k)$. The solid black lines are the linear combination functions whilst the light and the dashed lines are the partial structure factors weighted by A, B or C and the function carrying its full weight (in equation (5.4)).

pair $j'k'$). Thus,

$$\begin{aligned} d_{j'k'}(k) &= f_{j'}(k) f_{k'}(k) \left\{ \sum_i^{uc} b_i \right\}^2 F^{\mathrm{nd}}(k) \\ &\quad - b_{j'} b_{k'} \left\{ \sum_i^{uc} f_i(k) \right\}^2 F^{\mathrm{xrd}}(k), \\ &= f_{j'}(k) f_{k'}(k) \sum_i \sum_j^{uc} b_i b_j S_{ij}(k) \\ &\quad - b_{j'} b_{k'} \sum_i \sum_j^{uc} f_i(k) f_j(k) S_{ij}(k), \\ &= \sum_{jk \neq j'k'} \left\{ f_{j'}(k) f_{k'}(k) b_j b_k - b_{j'} b_{k'} f_j(k) f_k(k) \right\} S_{jk}(k), \end{aligned} \tag{5.2}$$

where the summations are over the molecular formula unit[3]. In addition, functions of the form

$$d^{j''k''}_{j'k'}(k) = \frac{d_{j'k'}(k)}{f_{j'}(k) f_{k'}(k) b_{j''} b_{k''} - b_{j'} b_{k'} f_{j''}(k) f_{k''}(k)}, \tag{5.3}$$

are defined, which effectively normalize $d_{j'k'}(k)$. In [48] the three functions considered are

$$\begin{aligned} d^{\mathrm{ClCl}}_{\mathrm{ZnZn}}(k) &= A S_{\mathrm{ZnCl}} + S_{\mathrm{ClCl}}, \\ d^{\mathrm{ClCl}}_{\mathrm{ZnCl}}(k) &= B S_{\mathrm{ZnZn}} + S_{\mathrm{ClCl}}, \\ d^{\mathrm{ZnZn}}_{\mathrm{ClCl}}(k) &= C S_{\mathrm{ZnCl}} + S_{\mathrm{ZnZn}}, \end{aligned} \tag{5.4}$$

where

$$\begin{aligned} A &= \frac{f^2_{\mathrm{Zn}}(k) b_{\mathrm{Zn}} b_{\mathrm{Cl}} - b^2_{\mathrm{Zn}} f_{\mathrm{Zn}}(k) f_{\mathrm{Cl}}(k)}{f^2_{\mathrm{Zn}}(k) b^2_{\mathrm{Cl}} - b^2_{\mathrm{Zn}} f^2_{\mathrm{Cl}}(k)}, \\ B &= \frac{f_{\mathrm{Zn}}(k) f_{\mathrm{Cl}}(k) b^2_{\mathrm{Zn}} - b_{\mathrm{Zn}} b_{\mathrm{Cl}} f^2_{\mathrm{Zn}}(k)}{f_{\mathrm{Zn}}(k) f_{\mathrm{Cl}}(k) b^2_{\mathrm{Cl}} - b_{\mathrm{Zn}} b_{\mathrm{Cl}} f^2_{\mathrm{Zn}}(k)} \\ C &= \frac{f^2_{\mathrm{Cl}}(k) b_{\mathrm{Zn}} b_{\mathrm{Cl}} - b^2_{\mathrm{Cl}} f_{\mathrm{Zn}}(k) f_{\mathrm{Cl}}(k)}{f^2_{\mathrm{Cl}}(k) b^2_{\mathrm{Zn}} - b^2_{\mathrm{Cl}} f^2_{\mathrm{Zn}}(k)}, \end{aligned} \tag{5.5}$$

[3] Note that the $jk = j'k'$ term could be kept in the last equation, but is zero.

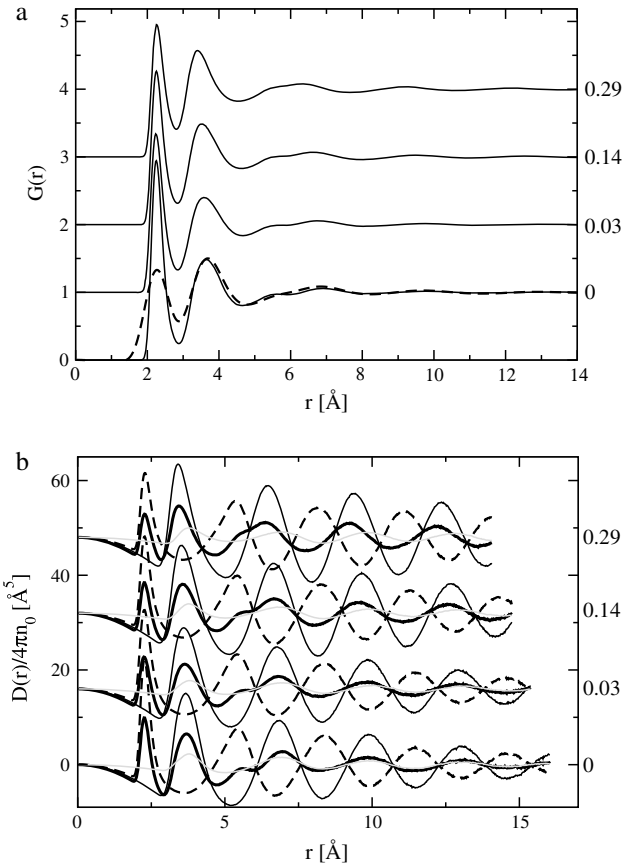

Figure 5. (a) Total neutron pair distribution functions, $G^{\mathrm{nd}}(r)$, calculated as a function of pressure (shown on the right-hand side in GPa). For the zero pressure functions, the dashed line represents the function calculated via Fourier transform of the total scattering function shown in figure 2(a). (b) Pair distribution function, $D(r)$, with the weighted partial pair distribution function contributions. Key: thick black line— $D(r)$, thin black line—$g_{\mathrm{ClCl}}(r)$ contribution, dashed line—$g_{\mathrm{ZnCl}}(r)$ contribution, light line—$g_{\mathrm{ZnZn}}(r)$ contribution.

and where $A = 0.402$, $B = -0.740$ and $C = 0.543$, assuming the x-ray form factor to be invariant with scattering angle ($f(k) = f(0)$). Figure 4 shows these three functions along with the (weighted) breakdowns in terms of respective pair of partial structure factors. Both $d^{\mathrm{ClCl}}_{\mathrm{ZnZn}}(k)$ and $d^{\mathrm{ClCl}}_{\mathrm{ZnCl}}(k)$ appear similar to those obtained from experiment (figure 5 in [48]). For $d^{\mathrm{ClCl}}_{\mathrm{ZnCl}}(k)$ the simulated function shows a small indentation at $k \sim 1$ Å^{-1}, reflecting the negative contribution of $S_{\mathrm{ZnZn}}(k_{\mathrm{FSDP}})$, whilst the experimentally-obtained function shows a small maximum at the same scattering angle. It is clear, however, that these features arise from the subtle interplay of the two underlying partial structure factors which near-cancel in this k region. Analogous comments apply to $d^{\mathrm{ZnZn}}_{\mathrm{ClCl}}(k)$, which shows a significant difference between the simulated and experimental functions at $k \sim 2$ Å^{-1} (i.e. in the region associated with the principal peak). In the experimentally-obtained function the feature at $k \sim k_{\mathrm{PP}}$ appears as a trough whilst in the simulated function it appears as a peak. Again, however, this feature arises from the near-cancellation of the principal peaks in $S_{\mathrm{ZnCl}}(k)$ and $S_{\mathrm{ZnZn}}(k)$.

Figure 5(a) shows the total neutron pair distribution functions, $G^{\rm nd}(r)$, for the four pressures. The ambient pressure peak positions are consistent with those observed experimentally [15, 46]. The relative intensities of the first and second peaks are more consistent with the earlier studies of Allen *et al* [15] rather than the later studies of Pfleiderer *et al* [46]. This difference in relative intensity may simply be an artefact of the Fourier transform procedure, as the nature of the two experiments (the latter being performed in a pressure cell) led to significantly greater probed scattering angle range in the older experiments (and hence more reliable transforms to real space). To emphasize this point figure 5(a) also shows the zero pressure $G^{\rm nd}(r)$ calculated by the Fourier transformation of the total scattering function shown in figure 2(a). The relative peak intensities in the transformed function are much more in keeping with the later experimental results [46]. It is worth stressing, however, that such issues affect peak intensities and not positions, although the former may be significant if considering the ion coordination environments.

In order to emphasize pressure-driven changes in structure on an intermediate length-scale, figure 5(b) shows the pair distribution function, $D(r) = 4\pi n_0 r^2(G(r) - 1)$. It is clear that subtle changes in the range 6–8 Å identified experimentally [46] arise from subtle changes in the relative phases of the underlying partial ion–ion pair distribution functions. To emphasize this, figure 6 shows the evolution of the (unweighted) partial pair distribution functions, $g_{\alpha\beta}(r)$, as a function of pressure. The origin of the subtle changes in $G^{\rm nd}(r)$ in the $r \sim$ 6–8 Å region is clear (highlighted by the arrow on the figure on the high pressure curves). The pressure-driven change in the Cl–Cl distribution function consists of a shift of the nearest-neighbour peak to lower r, coupled with a reduction on the length-scale of the r-space oscillations. In the $r \sim$ 6–8 Å region at low pressure $g_{\rm ClCl}(r)$ and $g_{\rm ZnZn}(r)$ are near in phase and out of phase with $g_{\rm ZnCl}(r)$. As the pressure is increased, however, this simple phase relationship breaks down. The experimentally-observed changes in the IRO on application of pressures up to ∼0.3 GPa can be understood in terms of the compressibilities of the respective anion and cation sub-lattices. At zero pressure the network is dominated by four-coordinate cations ($n_4 = 0.75, n_5 = 0.25$, where n_α is the fraction of cation sites with coordination number α). On application of a small external pressure the system remains dominated by approximately four-coordinate cations, but with a significant minority of five-coordinate species (and hence a rise in the mean cation–anion coordination number). The increase in the number of five-coordinate species corresponds to the shift in the first peak in $g_{\rm ClCl}(r)$ to lower r (i.e. the anion sublattice becomes more compressed—figure 6). The position of the first peak in $g_{\rm ZnCl}(r)$ shifts to lower r on initial application of pressure, then to larger r as the applied pressure is further increased. These changes reflect an initial reduction in the Zn–Cl bond length at approximately constant coordination number, followed by an increase in the mean cation–anion coordination number (with an associated rise in the mean cation–anion nearest-neighbour length-scale). These shifts act to control the form of the total pair distribution function in the intermediate-range as they lead to subtle phase shifts in the underlying contributing pair distribution functions.

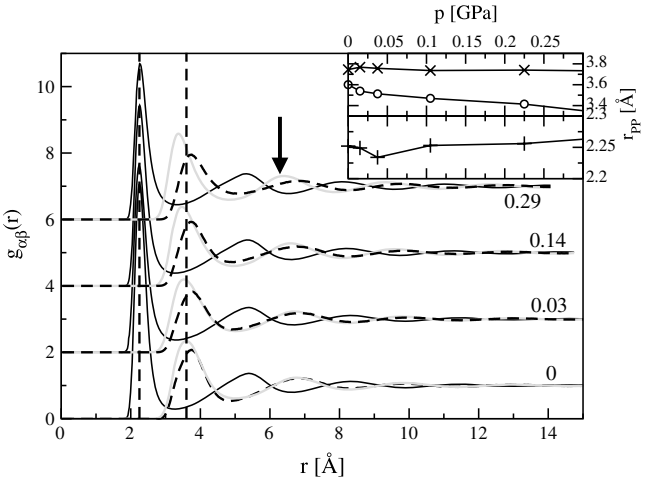

Figure 6. (Main panel) Partial pair distribution functions, $g_{\alpha\beta}(r)$, calculated at four pressures (indicated on the right-hand side in GPa). Key: solid black line—$g_{\rm ZnCl}(r)$, dashed line—$g_{\rm ZnZn}(r)$, light line-$g_{\rm ClCl}(r)$. The insets show the pressure evolution of the first peak positions in the three functions. Key: +—$g_{\rm ZnCl}(r_{\rm PP})$, ×—$g_{\rm ZnZn}(r_{\rm PP})$, ○—$g_{\rm ClCl}(r_{\rm PP})$.

5.2. Polyamorphic behaviour

In order to probe any potential polyamorphic behaviour, additional pressurization simulations are performed at low temperature ($T < T_{\rm m}$) and over a greater pressure range than those considered previously, to $p \sim 3$ GPa. A molten state configuration is cooled to 100 K using the Nosé–Hoover thermostats and then further simulations are performed at 100 K intervals in the range 100–600 K in which the pressure is increased by ∼0.3 GPa every 100 ps. Further simulations are performed in which the high pressures are released using a pressure change of ∼−0.3 GPa, again every 100 ps. It is important to emphasize that the cooling rates used are way in excess of those accessible experimentally. As a result, the low temperature structures accessed will reflect the high temperature (liquid state) structures far more than in the real glasses. However, in the present work we are primarily interested in potential pressure-driven structural changes (i.e. potential LDA ⟶ HDA transformations). As a result, it is reasonable to assume that any observed changes induced by pressure changes may be at least indicative of those observable for a real glass. An analogous set of simulations has been performed to probe the LDA ⟶ HDA transformations in amorphous Si [67].

Figure 7 shows the approximate LDA/HDA coexistence curve, superimposed on the phase diagram constructed by Brazhkin *et al* [42]. The approximate LDA/HDA coexistence is identified as intermediate between the increasing and decreasing pressure simulation transitions (which we associate with the respective spinodal lines and are identified from large volume changes observed in the respective pressure–volume curves). The volume change on transition is of the order of $\Delta V \sim 1.8$ cm^3 mol^{-1}, which, coupled with the gradient in figure 7, corresponds to and entropy change for the LDA ⟶ HDA transformation of $\Delta S \sim 1.6$ J K^{-1} mol^{-1}.

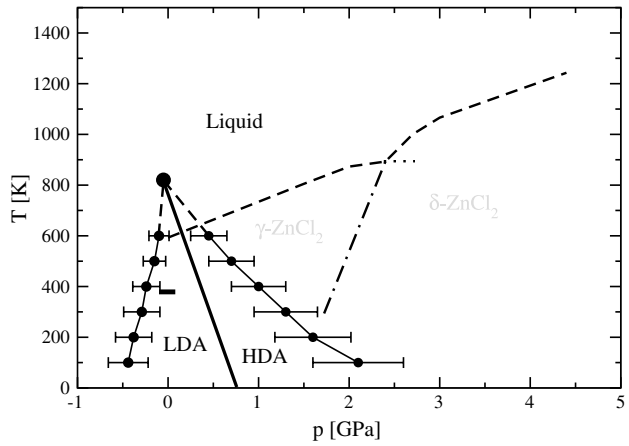

Figure 7. Approximate phase diagram for $ZnCl_2$. The dashed line represents the melting curve identified by Brazhkin *et al* [42]. The dot–dashed line indicates the location of the γ-$ZnCl_2 \longrightarrow \delta$-$ZnCl_2$ pressure-driven phase transformation. The thin solid lines (with solid circles) shows the approximate locations of the increasing and decreasing pressure spinodals. The solid line (determined from the pair of spinodals) shows the approximate location of the LDA/HDA phase boundary and leads to an approximate critical point (large filled circle). The short dashed horizontal line indicates the glass transition temperature at ambient pressure.

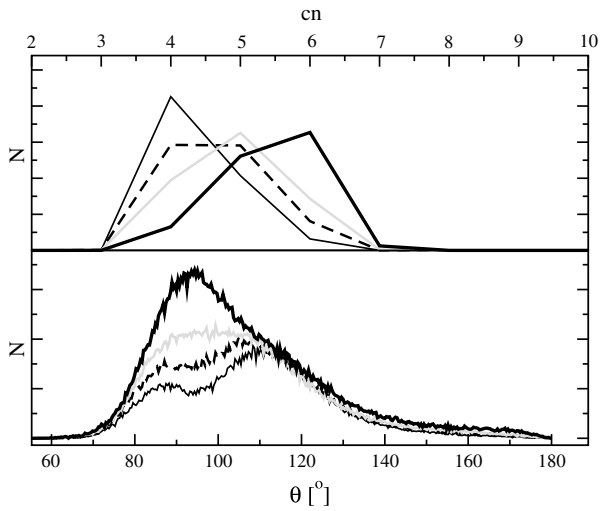

Figure 8. (Upper panel) cation–anion coordination number distributions and (lower panel) Zn–Cl–Zn bond angle distributions at four pressures along the $T = 600$ K isotherm. Key: thin solid line—zero pressure, dashed line—0.6 GPa, light line—0.9 GPa, thick solid line—1.5 GPa.

At the elevated pressures which correspond to the proposed LDA $\longrightarrow$ HDA pressure-driven phase transition, the changes in structure are more dramatic than those noted in the previous section. Figure 8 shows the cation coordination distributions at four pressure along with the corresponding Zn–Cl–Zn bond angle distributions. At low pressure the bond angle distribution displays a major peak at $\sim$110° and a side peak at $\sim$88°, corresponding to the presence of corner- and edge-sharing inter-tetrahedral connections respectively. The corner- and edge-sharing units can be effectively quantified by counting the number of four membered rings (each of which corresponds to an edge-sharing unit). At ambient pressures the fraction of cation sits in pure edge-sharing environments varies from $\sim$0.27 at 600 K to $\sim$0.36 at 100 K. The reduction in the number of edge-sharing units as the temperature increases reflects their role as effective intermediate structures for local environments to transform between local corner-sharing environments. At high temperatures the activation barriers to these motions are more readily overcome and hence fewer edge-sharing units are observed. As the number of five- and six-coordinate cation environments increases with pressure, the number of edge-sharing units increase in order to accommodate the greater local coordination whilst maintaining the fixed stoichiometry. On crossing the proposed coexistence curve (figure 7) the number of five- and six-coordinate cations jump significantly and the bond angle distribution changes from the characteristic two-peak function into a function with a single peak. The LDA $\longrightarrow$ HDA transformation is, therefore, associated with a change from a structure dominated by four-coordinate cation sites, to a structure dominated by six-coordinate cations. Similar coordination environment changes have been observed for SiO_2 [35].

Although $ZnCl_2$ can be classified, at ambient pressure, as a tetrahedral network system (and therefore grouped with systems as diverse as Si, H_2O, SiO_2, GeO_2, $BeF_2, \ldots$) the proposed phase diagram shows some interesting potential differences. The calculated critical temperature ($T_c \sim 825$ K) is greater than the glass transition temperature ($T_g \sim 375$ K), which is analogous to the observation for H_2O ($T_c \sim 194$ K, $T_g \sim 136$ K) but different to that observed for SiO_2 ($T_c \sim 730$ K, $T_g \sim 1450$ K (see [35] and references therein)). Furthermore, the predicted critical temperature is higher than the melting point ($T_m \sim 591$ K) which is different to both H_2O and SiO_2, but similar to the behaviour predicted for elemental carbon [68]. In addition, this prediction is consistent with the system thermodynamics. Within a two-state model [70, 69] a critical temperature of 825 K corresponds to a non-ideal mixing parameter, W ($\equiv 2RT_c$), of $\sim$13.7 kJ mol^{-1}. Most systems would be expected to show $T_c < T_m$ reflecting the relative magnitudes of the enthalpies of melting and that associated with the LDA $\longrightarrow$ HDA transition. However, $ZnCl_2$ is recognized as anomalous in the sense that the observed enthalpy of melting is relative low (16.1 kJ mol^{-1} [71], 9.8 kJ mol^{-1} [72]) which is of the same order as typical LDA/HDA enthalpy changes. As would be expected, our predicted entropy change ($\Delta S \sim 1.6$ J K^{-1} mol^{-1}) is significantly smaller than that associated with melting ($\Delta S \sim 16.6$ J K^{-1} mol^{-1} [72]). Future work will focus on these predicted properties as a function of the potential model in order to understand the factors which control these inherent transition temperatures.

6. Summary and conclusions

In summary, a potential model has been developed which is based on a relatively simple ionic effective pair potential approach, but which contains a description of many-body interactions which arise from the (anion) polarization. The

inclusion of anion polarization is critical if the experimentally-observed nearest-neighbour Zn–Zn separation is to be reproduced using physically transparent potential parameters. The model reproduces a range of static structural properties, notably the presence of the first-sharp diffraction peak at scattering angles corresponding to $k \sim 1$ Å^{-1}. Furthermore, both the pressure- and temperature-dependent behaviour of this feature are reproduced.

Exploratory calculations, in which a (very rapidly cooled) glass is generated from the simulated liquid, indicates the presence of a pressure-driven phase transformation between low- and high-density amorphous configurations. These states are characterized by differences in both the nearest-neighbour and intermediate-range environments. The critical temperature for the LDA/HDA coexistence is predicted to lie above the system melting point, consistent with the anomalously low enthalpy of melting.

Acknowledgments

The authors thank Professor Philip Salmon (Department of Physics, University of Bath) and Professor Paul F McMillan (Department of Chemistry, University College London) for useful discussions.

References

[1] Hansen J-P and McDonald I R 1986 *Theory of Simple Liquids* (New York: Academic)
[2] Ubbelohde A R 1978 *The Molten State of Matter* (New York: Wiley)
[3] Rovere M and Tosi M P 1986 *Rep. Prog. Phys.* **49** 1001
[4] March N H and Tosi M P 1984 *Coulomb Liquids* (New York: Academic)
[5] Wilson M and Madden P A 1997 *Mol. Phys.* **92** 197–210
Wilson M and Ribero M C C 1999 *Mol. Phys.* **96** 867–76
[6] Massobrio C, van Roon F H M, Pasquarello A and De Leeuw S W 2000 *J. Phys.: Condens. Matter* **12** L697
Massobrio C, Pasquarello A and Car R 1998 *Phys. Rev. Lett.* **80** 2342
Massobrio C, Pasquarello A and Car R 2001 *Phys. Rev.* B **64** 144205
Massobrio C and Pasquarello A 2001 *J. Chem. Phys.* **114** 7976
Massobrio C and Pasquarello A 2003 *Phys. Rev.* B **68** 020201(R)
Massobrio C, Celino M and Pasquarello A 2004 *Phys. Rev.* B **70** 174202
Massobrio C and Pasquarello A 2007 *Phys. Rev.* B **75** 014206
[7] Cobb M, Drabold D A and Cappelletti R L 1996 *Phys. Rev.* B **54** 12162
Cobb M and Drabold D A 1997 *Phys. Rev.* B **56** 3054
Durandurdu M and Drabold D A 2002 *Phys. Rev.* B **65** 104208
Biswas P, Tafen D N and Drabold D A 2005 *Phys. Rev.* B **71** 054204
[8] Vashishta P, Kalia R K, Antonio G A and Ebbsjö I 1989 *Phys. Rev. Lett.* **62** 1651
Iyetomi H, Vashishta P and Kalia R K 1991 *Phys. Rev.* B **43** 1726
[9] Penfold I T and Salmon P S 1991 *Phys. Rev. Lett.* **67** 97
[10] Petri I, Salmon P S and Fischer H E 2000 *Phys. Rev. Lett.* **84** 2413
[11] Salmon P S and Petri I 2003 *J. Phys.: Condens. Matter* **15** S1509
[12] Sharma B K, Wilson M and Massobrio C M 2008 *J. Chem. Phys.* submitted
[13] Desa J A E, Wright A C, Wong A C and Sinclair R N 1982 *J. Non-Cryst. Solids* **51** 57
[14] Biggin S and Enderby J E 1981 *J. Phys. C: Solid State Phys.* **14** 3129
[15] Allen D A, Howe R A, Wood N D and Howells W S 1991 *J. Chem. Phys.* **94** 5071
[16] Salmon P S, Martin R A, Mason P E and Cuello G J 2005 *Nature* **435** 75
[17] Neuefeind J 2001 *Phys. Chem. Chem. Phys.* **3** 3987
[18] Madden P A and Wilson M 1996 *Chem. Soc. Rev.* **25** 339
[19] Wilson M and Madden P A 1994 *Phys. Rev. Lett.* **72** 3033
Wilson M and Madden P A 1998 *Phys. Rev. Lett.* **80** 532
[20] Foley M, Wilson M and Madden P A 1995 *Phil. Mag.* B **71** 557
[21] Wilding M C, Wilson M and McMillan P F 2006 *Chem. Soc. Rev.* **35** 964
McMillan P F, Wilson M, Wilding M C, Daisenberger D, Mezouar M and Greaves G N 2007 *J. Phys.: Condens. Matter* **19** 415101
[22] Ponyatovsky E G and Barkalov O I 1992 *Mater. Sci. Rep.* **8** 147–91
[23] Debenedetti P G 1997 *Metastable Liquids* (Princeton, NJ: Princeton University Press)
[24] Brazhkin V V, Buldyrev S V, Ryzhov V N and Stanley H E 2002 *New Kinds of Phase Transition: Transformations in Disordered Substances* (Dordrecht: Kluwer)
[25] Tanaka H 2000 *Phys. Rev.* E **62** 6968
[26] Greaves G N and Sen S 2007 *Adv. Phys.* **56** 1
[27] Mishima O, Calvert L D and Whalley E 1985 *Nature* **314** 76
[28] Loerting T and Giovambattista N 2006 *J. Phys.: Condens. Matter* **18** R919–77
[29] Grimsditch M 1984 *Phys. Rev. Lett.* **52** 2379
[30] Smith K H, Shero E, Chizmeshya A and Wolf G H 1995 *J. Chem. Phys.* **102** 6851
[31] Sampath S, Benmore C J, Lantzky K M, Neuefeind J, Leinenweber K, Price D L and Yarger J L 2003 *Phys. Rev. Lett.* **90** 115502
[32] Wright A C, Bachra B, Brunier T M, Sinclair R N, Gladden L F and Portsmouth R L 1992 *J. Non-Cryst. Solids* **150** 69
[33] Galeener F L 1985 *J. Non-Cryst. Solids* **75** 399
[34] Devine R A B, Dupree R, Farnan I and Capponi J J 1987 *Phys. Rev.* B **35** 2560
[35] Saika-Voivod I, Sciortino F and Poole P H 2000 *Phys. Rev.* E **63** 011202
[36] Triolo R and Narten A H 1981 *J. Chem. Phys.* **74** 703
[37] Wong J and Lytle F W 1980 *J. Non-Cryst. Solids* **37** 273
[38] Price D L, Saboungi M-L, Susman S, Volin K J and Wright A C 1991 *J. Phys.: Condens. Matter* **3** 9835
[39] Imaoka M, Konagaya Y and Hasegawa H 1971 *J. Ceram. Soc. Japan* **69** 97
[40] Sinclair R, Desa J A E, Etherington G, Johnson P A V and Wright A C 1980 *J. Non-Cryst. Solids* **42** 107
[41] Fillaux C, Couzinet B, Dreyfus C, Iti J P and Polian A 2005 *Phys. Scr.* T **115** 339–41
[42] Brazhkin V V, Lyapin A G, Popova S V, Katayama Y, Saitoh H and Utsumi W 2007 *J. Phys.: Condens. Matter* **19** 246104
[43] Sakai M, Kuroda N and Nishina Y 1985 *J. Phys. Soc. Japan* **54** 4081
[44] Polsky C H, Martinez L M, Leinenweber K, VerHelst M A, Angell C A and Wolf G H 2000 *Phys. Rev.* B **61** 5934
[45] Heusel G, Bertagnolli H, Kreitmeir M, Neuefeind J and Lemke A 2002 *Phys. Chem. Chem. Phys.* **4** 4155
[46] Pfleiderer T, Waldner I, Bertagnolli H, Tödheide K and Fischer H E 2003 *Phys. Chem. Chem. Phys.* **5** 5313
[47] Soper A K 2005 *Phys. Rev.* B **72** 104204
[48] Neuefeind J, Tödheide K, Lemke A and Bertagnolli H 1998 *J. Non-Cryst. Solids* **224** 205

[49] Woodcock L V, Angell C A and Cheeseman P 1976 *J. Chem. Phys.* **65** 1565
[50] Gardner P J and Heyes D M 1985 *Physica* B **131** 227
[51] Kumta P N, Deymier P A and Risbud S H 1986 *Physica* B+C **153** 85–92
[52] Pyper N C, Pike C G, Popelier P and Edwards P P 1995 *Mol. Phys.* **86** 995
[53] Pyper N C 1991 *Adv. Solid-State Chem.* **2** 223
[54] Riberio M C C, Wilson M and Madden P A 1998 *J. Chem. Phys.* **108** 9027
Riberio M C C, Wilson M and Madden P A 1998 *J. Chem. Phys.* **109** 9859
Riberio M C C, Wilson M and Madden P A 1999 *J. Chem. Phys.* **110** 4083
[55] Bassen A, Lemke A and Bertagnolli H 2000 *Phys. Chem. Chem. Phys.* **2** 1445
[56] Huang S, Yoshida F and Wang W 2004 *J. Mol. Liq.* **115** 81
[57] Sharma B K and Wilson M 2006 *Phys. Rev.* B **73** 060201
[58] Fowler P W and Madden P A 1985 *Phys. Rev.* B **31** 5443
T̈emmer P, Fowler P W, Wilson M and Madden P A 1999 *J. Chem. Phys.* **111** 2038
Domene C, Fowler P W, Madden P A, Xu J, Wheatley R J and Wilson M 2001 *J. Phys. Chem.* A **105** 4136
[59] Wilson M, Madden P A, T̈emmer P, Fowler P W, Batana A, Bruno J, Munn R W and Monard M C 1999 *Mol. Phys.* **96** 1457
[60] Domene C, Fowler P W, Wilson M, Madden P A and Wheatley R J 2002 *Chem. Phys. Lett.* **333** 403
[61] Nosé S and Klein M L 1983 *Mol. Phys.* **50** 1055
[62] Martyna G J, Tobias D J and Klein M L 1994 *J. Chem. Phys.* **101** 4177
[63] Klemm W 1926 *Z. Anorg. Chem.* **152** 235
[64] Duke F R and Fleming R A 1957 *J. Electrochem. Soc.* **104** 251
[65] Sears V F 1992 *Neutron News* **3** 26
[66] Cromer D T and Waber J T 1974 *International Tables for X-ray Crystallography* ed J A Ibers and W C Hamilton (Birmingham: Kynoch) p 71
[67] Daisenberger D, Wilson M, McMillan P F, Quesada Cabrera R, Wilding M C and Machon D 2007 *Phys. Rev.* B **75** 224118
[68] Ponyatovsky E G 2003 *J. Phys.: Condens. Matter* **15** 6123
[69] Strässler S and Kittel C 1965 *Phys. Rev.* A **139** 758
[70] Rapoport E 1967 *J. Chem. Phys.* **46** 2891
[71] Kubaschewski O, Alcock C B and Spencer P J 1993 *Materials Thermochemistry* (Oxford: Pergamon)
[72] Angell C A, Williams E, Rao K J and Tucker J C 1977 *J. Phys. Chem.* **81** 238